International Core Journal of Engineering Volume 7 Issue 8, 2021
ISSN: 2414-1895 DOI: 10.6919/ICJE.202111_7(11).0022

Simulated rotor assembly deviation prediction based on PCA-BP neural network

Jianyu Fan, Cong Yue and Long Liu

Logistics Engineering College, Shanghai Maritime University, Shanghai 201306, China.

Abstract

Aeroengine high-pressure rotor has a typical bolt connection structure. Mechanical properties of bolted components greatly affect the performance and stability of whole engine structural system. In this paper, the first two critical speeds of a rotor were calculated through finite element analysis, and a bolt assembly deviation test was designed and carried out. Based on the experimental results, a neural network prediction model was established, and the principal component analysis(PCA) method was used to reduce the complexity of the data. By applying PCA method the average error is reduced from 12.63% to 4.62%. With this prediction model, the location of bolt assembly deviation could be effectively determined by using specific frequency response peak and amplitude.

Keywords

High-pressure rotor, Neural Network, PCA, Assembly deviation, Predictive Model.

1. Introduction

Aero-engine assembly is the terminal and core part of manufacturing process[1-2]. In an aero-engine assembly process, the quality of the high-pressure rotor assembly determines the performance of the entire aero-engine. Problems arising from the overall assembly of the high-pressure rotor will be accumulated with the assembly process, so the quality and precision in the assembly process are the guarantee of the quality of the aero-engine products.

The fit of the mounting side of the aero-engine high-pressure rotor is primarily a bolt-stop fit. Luo Wendong [3] investigated the relationship between the bolt preload force and the dynamic and static stiffness, critical speed, and dynamic response characteristics of the rotor system in the aero-engine rotor. Hong, J. et al[4]concluded that under rotor bending deformation, the connection interface stiffness loss is significant, which will greatly reduce the rotor bending critical speed. Yang[5]used the flush coordinate change method to establish a mathematical model for analyzing the error transmission of aero-engine rotors, based on the assembly phase in the model to make the geometric coaxiality of the rotor assembly to meet the assembly requirements. Chen xuefeng et al [6] established a method to detect the assembly performance of aero-engine, which used vibration sensors and signal acquisition system to obtain the vibration response signal of aero-engine, and then extracted the impulse response sub-signal to extract the average assembly performance index so as to judge the assembly quality. Zou et al[7]studied the effects of different lubricants and different lubrication methods on the torsion-tension relationship of bolt connection and the number of bolt tightening Macmillan et al [8] used several sub-test systems to analyze the stress signals at different positions of the rotor and obtained the effect of tolerance parameters of the rotor on the assembly quality. Yi Chaogao[9]established a rotor elastic stacking model and optimized the rotor coaxiality phase built on genetic algorithm. Li Yuqi et al [10-11] established a nonlinear rotor system dynamics model considering the gyroscopic moment and the initial deformation due to the uneven bolt preload force, analyzed the effect of different initial deformation and bearing clearance on the nonlinear vibration

ISSN: 2414-1895 DOI: 10.6919/ICJE.202111_7(11).0022

characteristics of the rotor system, and verified the accuracy of the obtained conclusions through experiments. Tuckmantel [12] summarized the vibration signatures resulting from coupling misalignments. Ebrahimi et al. [13] investigated a magnetically supported flexible rotor system with auxiliary bearings.Yan Qiang [14] established a simplified model of the bolted rotor considering the connection structure, initially investigated the effect of assembly tightness on the inherent frequency of the bolted rotor, and proposed a bolted rotor assembly tightness detection method based on wavelet energy entropy, and verified the correctness of the method through experiments. Zhao [15-16] assessed the time-varying stiffness of the joint caused by bolt loosening and its influence on the steady-state response of the rotor.

At present, the research on rotor assembly deviation mostly focuses on the geometric relationship between the connecting structures, There is a lack of combined analysis between the overall dynamic response characteristics of the connecting structure and the influence of multi bolt assembly performance. In order to identify the variation characteristics of the bolt connection error of high pressure rotor on the overall dynamic response, a prediction model of bolt assembly deviation based on simulating the dynamic response of high pressure rotor is introduced. A prediction model of bolt assembly deviation was established by combining experimental research with neural network.

2. Analysis of aeroengine rotor dynamics

2.1 Finite element model

The experimental objective of this experiment is a scaled-down model of an aero-engine core. The simulated rotor simulates the three main structural components of the aeroengine high-pressure rotor: the advanced compressor, the combustion chamber and the high-pressure turbine. The whole rotoe has 5 mounting edges, and each mounting edge has 24 or 36 M6 bolts symmetrically connected with a tightening torque controlled at 8 Nm, and the stop has an overrun of 0.01 mm or more.

In this paper, Timoshenko beam cells are used to analyze the simulated rotor of an aero-engine, as showed in Figure 1. The simulated rotor model has 101 nodes and 100 beam cells with 6 degrees of freedom at each node. The disk is right on nodes 14, 19, 21, 26, 29 and 39, and the bearing is at nodes 3 and 49. The bearing stiffness is isotropic, and the support stiffness of pivot 1 is 9.5×10^6 N/m, and that of pivots 2 is 1.6×10^7 N/m. The unevenness is at nodes 9, 29 and 39, and the size of unevenness is 200 $g \cdot mm$.

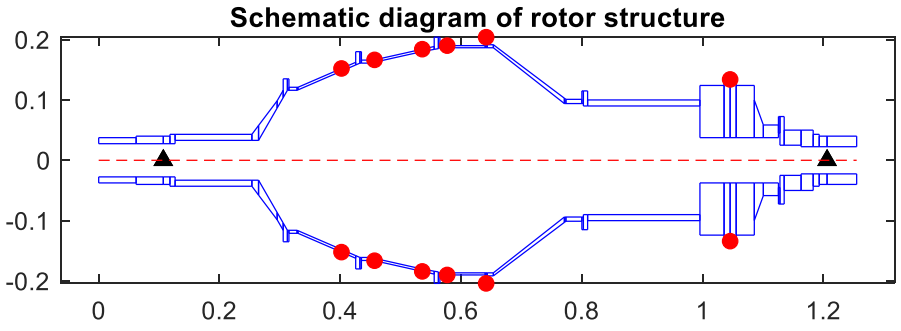

Figure 1. Aero-engine simulation rotor finite element model

2.2 Equations of motion of the system

The displacement vector for a rotor system with n nodes and n-1 shaft segments connected is:

$$\begin{cases} \{U_1\} = [x_1, \theta_{y1}, x_2, \theta_{y2}, \dots, x_n, \theta_{yn}] \\ \{U_2\} = [y_1, -\theta_{x1}, y_2, -\theta_{x2}, \dots, y_n, -\theta_{xn}] \end{cases} \quad (1)$$

Combining the equations of motion of the disc, the shaft segment and the bearing, the equation of motion of the system can be obtained as:

ISSN: 2414-1895 DOI: 10.6919/ICJE.202111_7(11).0022

$$\begin{cases}[M_1]\{\ddot{U}_1\} + \Omega[J_1]\{\dot{U}_2\} + [K_1]\{U_1\} = \{Q_1\} \\ [M_1]\{\ddot{U}_2\} - \Omega[J_1]\{\dot{U}_1\} + [K_1]\{U_2\} = \{Q_2\}\end{cases} \quad (2)$$

Where the mass matrix $[M_1]$ the slew matrix $\Omega[J_1]$ and the stiffness matrix $[K_1]$ are all symmetric sparse matrices with half bandwidth of order $2n \times 2n$.

When the bearing is isotropic, i.e. $k_{xx} = k_{yy}$ and $k_{xy} = k_{yx} = 0$. Ignoring the damping and the equivalent mass of the bearing seat, the system's differential equation of motion (Eq. 2) of the chi-squared form is:

$$\begin{cases}[M_1]\{\ddot{U}_1\} + \Omega[J_1]\{\dot{U}_2\} + [K_1]\{U_1\} = \{0\} \\ [M_1]\{\ddot{U}_2\} - \Omega[J_1]\{\dot{U}_1\} + [K_1]\{U_2\} = \{0\}\end{cases} \quad (3)$$

When the angular speed of rotation is given, from the frequency equation:

$$|-M_1\omega^2 + J_1\Omega\omega + K_1| = 0 \quad (4)$$

The $2N$ forward vortex and $2N$ reverse vortex frequencies can be found.

For isotropic bearings, the unbalanced response of the system can be obtained from equation (2) without accounting for the effects of damping and housing vibration, i.e:

$$\begin{cases}[M_1]\{\ddot{U}_1\} + \Omega[J_1]\{\dot{U}_2\} + [K_1]\{U_1\} = \Omega^2(\{Q_{1c}\}\cos\Omega t - \{Q_{2c}\}\sin\Omega t) \\ [M_1]\{\ddot{U}_2\} - \Omega[J_1]\{\dot{U}_1\} + [K_1]\{U_2\} = \Omega^2(\{Q_{2c}\}\cos\Omega t + \{Q_{1c}\}\sin\Omega t)\end{cases} \quad (5)$$

where the right-hand side of the equation is the generalized force representation of the unbalanced excitation. Let:

$$\{z\} = \{U_1\} + \{U_2\} \quad (6)$$

Then equation (5) can be written as

$$[M_1]\{\ddot{z}\} - i\Omega[J_1]\{\dot{z}\} + [K_1]\{z\} = \Omega^2 e^{i\Omega t} \quad (7)$$

Preposition,$\{Q\} = \{Q_{1c}\} + i\{Q_{2c}\} = \{Q_{1c}\} + \{Q_{2c}\}e^{i\frac{\pi}{2}}$.

The special solution of the unbalanced response can be obtained from equation (7) as:

$$\{z\} = \{A\}e^{i\Omega t} \quad (8)$$

Preposition,$\{A\} = \Omega^2[-M_1\omega^2 + J_1\Omega\omega + K_1]^{-1}\{Q\}$.

Through the above method, the first two critical speed of the simulated rotor system are 483.615 rpm and 898.218 rpm.

3. Vibration experiments and data extraction

3.1 Rotor vibration test

The main task of this experiment is to study the variation law of the simulated rotor response under the specified assembly deviation by simulating the vibration response of the rotor mounting side, using force hammer excitation. In the test with hammer excitation, 12 measurement points are used, 6 in the axial direction and 2 in the circumferential direction. The sensor layout diagram is shown in Figure 2.

This experiment focuses on the assembly deviation design of the fourth mounting edge, which has 24 bolts. Each bolt on the fourth mounting edge is calibrated with the position number, and the numbering order is the top bolt in the vertical direction is marked as bolt No. 1, and the numbering is clockwise against the heading, in order of 1#-24# bolts. The excitation method is force hammer excitation, and the excitation point is shown in Figure 2.

ISSN: 2414-1895 DOI: 10.6919/ICJE.202111_7(11).0022

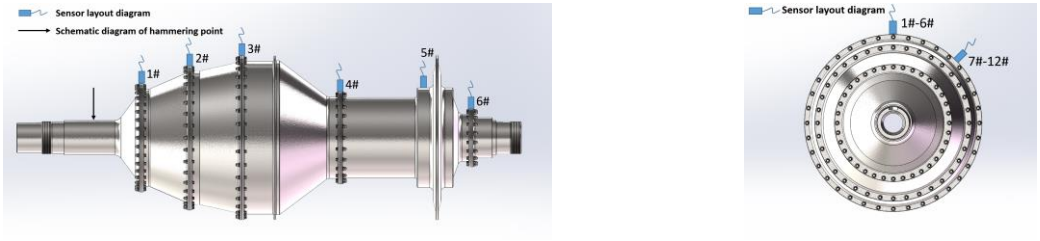

a) Front view b) Side view

Figure 2. Experimental scheme diagram

The experimental working conditions are: removing 1#-24# bolts in turn, striking of the hammering point and collecting vibration signals. The experimental diagram of bolt removal is shown in Figure 3.

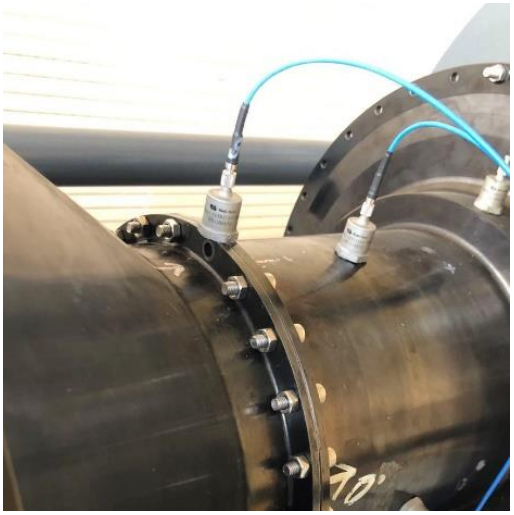

Figure 3. Experimental diagram of bolt removal

3.2 Data processing and extraction

After completing the force hammer excitation experiment, the spectrum analysis is performed and the vibration response curve is plotted. As showed in Figure 4, the vibration response curve plotted by the vibration signal measured by the uppermost sensor in the vertical direction under partial working conditions, the fourth installation side.

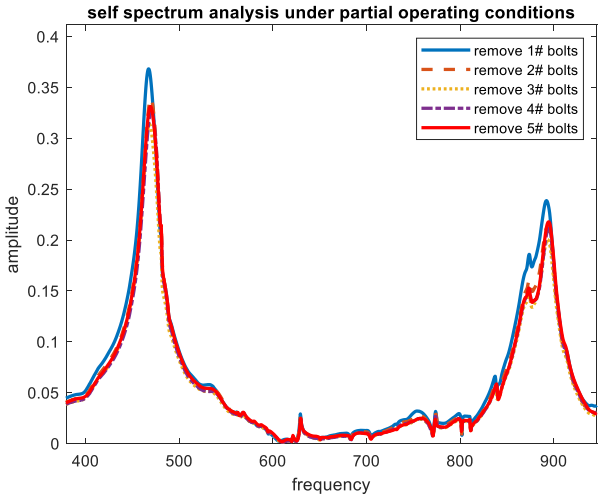

Figure 4. Partial schematic diagram of vibration response curve for some working conditions

Observation of the vibration response curve shows that the curve has obvious peaks near 470 Hz and 900 Hz, which correspond to the two frequencies calculated by the finite element model, so it is considered that the first two orders of bending frequencies of the simulated rotor are near 470 Hz

ISSN: 2414-1895 DOI: 10.6919/ICJE.202111_7(11).0022

and 900 Hz. The peak frequencies of the signals measured by the two sensors on the fourth mounting side and the corresponding amplitudes are extracted, as showed in Table 1:

Table 1. Peak frequency and amplitude

Work conditions	Frequency 1	Amplitude 1	Frequency 2	Amplitude 2	Frequency 3	Amplitude 3	Frequency 4	Amplitude 4
Dismantling 1#	467.343	0.369	892.500	0.239	468.281	0.228	892.031	0.157
Dismantling 2#	469.687	0.340	893.437	0.2139	470.625	0.215	893.437	0.142
Dismantling 3#	468.281	0.314	893.437	0.200	468.750	0.199	893.437	0.136
…	…	…	…	…	…	…	…	…
Dismantling 23#	465.468	0.326	892.500	0.236	466.875	0.214	892.031	0.175
Dismantling 24#	465.937	0.330	892.031	0.224	466.875	0.218	892.031	0.167

Table 1, frequency 1, amplitude 1, frequency 2, and amplitude 2 are the signals measured by the vertical sensor on the fourth mounting edge, and frequency 3, amplitude 3, frequency 4, and amplitude 4 are the signals measured by the sensor on the fourth mounting edge at an angle of 45 °to the vertical direction.

4. PCA-BP prediction model

4.1 BP Neural Network

BP neural network is a multilayer pre-feedback neural network, which consists of an input layer, hidden layer and output layer. BP neural network performs the following operations: first provide the training input data to the input layer neurons, then pass the signal layer by layer until the result of the output layer is produced, then calculate the error between the network output and the actual data output, then propagate the error backward to the hidden layer neurons, adjust the connection power and threshold of the hidden layer neurons by the error, and then iterate until the error requirement is met. BP neural network has the advantages of a clear model, simple structure and small computation, but also has some disadvantages, such as easy to fall into local minima, slow learning speed, etc.

The process of BP neural network prediction is to establish the training network first, then divide the data into training set and test set, use the training set to train the established network until the network meets the requirements, and then use the test set to test the trained network to check the training effect. The input layer of the BP neural network is 4 frequency values and 4 amplitude values with 8 parameters, and the output layer is the position of the removed bolt. The position of the removed bolt is represented by the radian system.

4.2 Principal component analysis

To improve the BP neural network prediction, a pre-processing method of the input data could be used. Principal component analysis is one of the most commonly utilized dimensionality reduction methods. The principle is to convert multidimensional variables into new variables with less correlation by means of dimensionality reduction. For problems with large amount of data and large linear correlation between data, principal component analysis can simplify the complex problems and retain the information of the original variables to the greatest extent while simplifying them, and they are not correlated with each other. The eight input parameters can be reduced by principal component analysis, and the reduced variables are used as the input of the BP neural network, and the prediction results are output by an iterative loop.

The mathematical model for principal component analysis is:

With a dimensional random vector consisting of p indicators.

$$X^0 = (x_1, x_2, \dots, x_p) \tag{9}$$

The composite indexes obtained are:

ISSN: 2414-1895 DOI: 10.6919/ICJE.202111_7(11).0022

$$\begin{cases} y_1 = (a_{11}x_1 + a_{21}x_2 + \cdots + a_{p1}x_p) \\ \vdots \\ y_p = (a_{1p}x_1 + a_{2p}x_2 + \cdots + a_{pp}x_p) \end{cases} \tag{10}$$

where, for $k = 1, \ldots, p$, we have:

$$\sum_{j=1}^{p} a_{jk}^2 = 1 \tag{11}$$

y_1 is the largest variance in the linear combination, and the other variables have decreasing variances according to the ordinal number and are uncorrelated with each other. Let $\lambda_1 \geq \lambda_2 \geq \cdots \geq \lambda_p$be the eigenvalues of the covariance array $D(X)$, then the contribution of the kth principal component is:

$$\frac{\lambda_k}{\sum_{j=1}^{p} \lambda_j} \tag{12}$$

The larger the cumulative contribution of the first m principal components, the smaller the information loss of the data.

The steps of principal component analysis are calculated as follows:

(1) Data standardization;

(2) Calculation of the covariance matrix of the standardized independent variable matrix;

(3) Compute the eigenvalue matrix and eigenvector matrix of the covariance matrix;

(4) Calculate the cumulative contribution of variables based on the eigenvalue matrix and eigenvector matrix;

(5) Principal components are selected instead of the original sample data.

The correlation coefficient matrix of each component (Table 2) and the eigenvalues of the correlation coefficient matrix are obtained from the principal component analysis to obtain the contribution of each component (Table 3). From Table 2, it can be seen that the four data sets of frequency 1 and frequency 3, amplitude 1 and amplitude 3, frequency 2 and frequency 4, and amplitude 2 and amplitude 4 have strong correlations. The principal component analysis method can avoid the problem of multicollinearity that may be brought by these factors with strong correlation. As can be seen from Table 3: the cumulative variance contribution of the first four principal components has been greater than 95%, meeting the requirement that the variance of the principal components accounts for more than 95% of the total variance. Therefore, through principal component analysis, the 8 components in the original data can be put into 4 principal components, so only the 1st to 4th principal components are needed to replace the original 8 components into the neural network.

Table 2. Correlation coefficient matrix between the components

Parameters	Frequency 1	Amplitude 1	Frequency 2	Amplitude 2	Frequency 3	Amplitude 3	Frequency 4	Amplitude 4
Frequency 1	1.000	0.442	0.271	0.109	0.970	0.505	0.280	-0.035
Amplitude 1	0.442	1.000	-0.517	0.689	0.352	0.895	-0.428	0.501
Frequency 2	0.271	-0.517	1.000	-0.453	0.342	-0.390	0.946	-0.417
Amplitude 2	0.109	0.689	-0.453	1.000	0.109	0.827	-0.350	0.860
Frequency 3	0.970	0.352	0.342	0.109	1.000	0.473	0.325	-0.058
Amplitude 3	0.505	0.895	-0.390	0.827	0.473	1.000	-0.328	0.613
Frequency 4	0.280	-0.428	0.946	-0.350	0.325	-0.328	1.000	-0.289
Amplitude 4	-0.035	0.501	-0.417	0.860	-0.058	0.613	-0.289	1.000

ISSN: 2414-1895 DOI: 10.6919/ICJE.202111_7(11).0022

Table 3. PCA analysis results

Parameters	Eigenvalue	Variance contribution rate (%)	Cumulative variance contribution (%)
PC1	3.916	48.950	48.950
PC2	2.633	32.915	81.865
PC3	0.982	12.270	94.136
PC4	0.246	3.076	97.211
PC5	0.133	1.665	98.877
PC6	0.046	0.580	99.457
PC7	0.028	0.356	99.812
PC8	0.015	0.188	100.000

4.3 PCA-BP neural network prediction

The four components of frequency 1, amplitude 1, frequency 2, and amplitude 2 in the above text are used as input factors, and the bolt removal location is used as the output factor to construct the neural network. In the process of constructing the BP neural network, the number of nodes in the hidden layer has a great influence on the prediction accuracy of the neural network. Too few nodes may lead to poor network training and low prediction accuracy; too many nodes will lead to more training time and overfitting of the network, so it is very important to determine the number of nodes in the hidden layer. Currently, the number of nodes in the hidden layer is mainly determined by the empirical formula.

$$l = \sqrt{m+n} + a \tag{13}$$

where m and n are the number of nodes in the input layer and the number of nodes in the output layer, respectively, and a is a constant between 1 and 10. In this paper, based on the above equation and the neural network test results, the number of nodes in the hidden layer is determined to be 6.

After determining the hidden layer nodes, the whole PCA-BP neural network model is constructed, and the modeling process is schematically described in Figure 5.

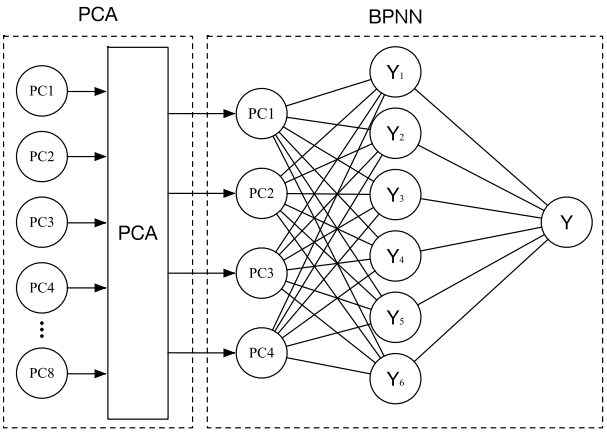

Figure 5. PCA-BP model

In order to compare and verify the effectiveness of PCA-BP neural network model, BP neural network model is established, and the same training group data are used to train the two models, and the results obtained after training are shown in Figure 6 and Table 4.

ISSN: 2414-1895 DOI: 10.6919/ICJE.202111_7(11).0022

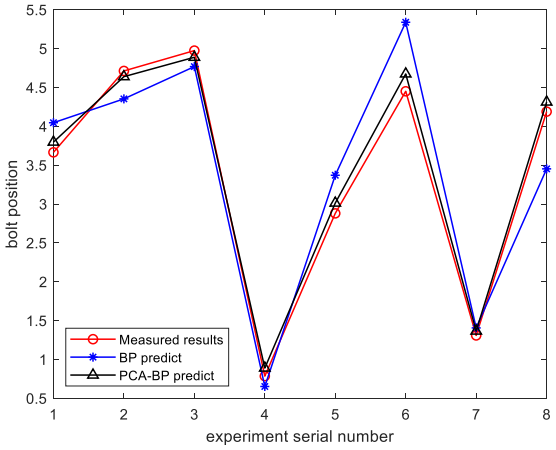

Figure 6. Model prediction curve

Table 4. Comparison of model predicted and measured values

No.	Missing bolt position	BP neural network prediction			PCA-BP neural network prediction		
		Predicted value	Prediction error	Relative error (%)	Predicted value	Prediction error	Relative error (%)
1	3.665	4.046	-0.381	10.394	3.797	-0.132	3.591
2	4.712	4.353	0.359	7.626	4.639	0.074	1.563
3	4.974	4.768	0.206	4.139	4.888	0.086	1.727
4	0.785	0.652	0.133	16.950	0.889	-0.104	13.223
5	2.880	3.370	-0.490	17.030	3.012	-0.132	4.600
6	4.451	5.339	-0.888	19.954	4.674	-0.224	5.024
7	1.309	1.406	-0.097	7.399	1.365	-0.056	4.307
8	4.189	3.453	0.736	17.577	4.313	-0.124	2.950

The relative error between the predicted and actual values of the bolt position by the BP neural network is calculated to be between 7.40% and 19.95%, with a difference of 12.56% and an average error of 12.63%; the absolute error is between -0.888 and 0.736. The relative error between the predicted and actual values of the bolt position by the PCA-BP neural network is between 1.56%-13.22%, with a difference of 11.66% and an average error of 4.62%; the absolute error ranged from -0.224-0.086. Comparing the two models, the overall change trend of the two models is basically the same and matches with the measured values. The maximum value of the relative error of the predicted data after the principal component analysis is smaller than the maximum value of the BP neural network prediction results, and the average relative error also has a significant reduction. It is proved that the prediction results after coupling PCA and BP neural network are better than the prediction results under the action of neural network alone, which proves the superiority of PCA-BP neural network prediction model.

5. Conclusion

In this paper, a PCA-BP neural network prediction model for the assembly deviation of the fourth mounting side of the simulated rotor of an aero-engine under hammering excitation conditions was developed, and the following main conclusions were obtained:

(1) The first two critical rotor speeds of 483.62 rpm and 898.22 rpm were calculated by the rotor dynamics finite element analysis method, and the simulated rotor vibration response curve of the aero-engine was verified to have peaks near 470 Hz and 900 Hz by hammering experiments;

ISSN: 2414-1895 DOI: 10.6919/ICJE.202111_7(11).0022

(2) After principal component analysed, the data complexity was reduced, the multicollinearity problem caused by strong correlation factors was avoided, and the number of inputted neurons of BP neural network was decreased. While ensuring the prediction accuracy of a neural network, the scale of the prediction model was effectively simplified. Comparing BP neural network model with PCA-BP neural network model, the average relative error of PCA-BP model was 4.62%, which was less than that of BP prediction model by 12.63%. It was proved that the accuracy of PCA-BP Neural Network model in simulating rotor assembly deviation prediction was higher than that of BP neural network model.

Acknowledgments

This work is supported by the innovation action plan project of Shanghai Science and Technology Commission (18BZ1100802)

References

[1] Sun Shanmin, Zhou Shuo, Gao Dove, Li Lin. Key technical issues of aero-engine assembly simulation[J]. Aviation manufacturing technology,2018,61(22):98-103.

[2] Sun Shanmin, Li Yong. Study on the influence of manufacturing error of aeroengine rotor mounting edge on assembly performance [J]. Modern manufacturing technology and equipment, 2020,56 (07): 126-131

[3] Luo W D, Tan M, Feng Y Q. Analysis of vibration control technology of aero-engine whole engine[J]. Science and Technology Information,2020,18(16):79-80.

[4] Hong J, Xu X.R., Su Z.M., Ma Y.H.. High-speed rotor connection structure stiffness loss and vibration characteristics[J]. Journal of Beijing University of Aeronautics and astronautics, 2019,45(01):18-25.

[5] Z. Yang et al. A probabilistic approach to variation propagation control for straight build in mechanical assembly[J]. The International Journal of Advanced Manufacturing Technology, 2013, 64(5-8) : 1029-1047.

[6] Chen Xuefeng, An aero-engine rotor assembly performance testing method. Shaanxi Province, Xi'an Jiaotong University, 2010-02-01.

[7] Zou Q , Sun T S , Nassar SA , et al. Effect of Lubrication on Friction and Torque-Tension Relationship in Threaded Fasteners[J]. Tribology Transactions, 2007, 50(1):127-136.

[8] Mcmillan A . System and method for improving the damage tolerance of a rotor assembly:, EP2525049[P]. 2012.

[9] Gao Yichao. Research on aero-engine rotor assembly accuracy prediction and phase optimization method [D]. Dalian University of Technology,2020.

[10] Li Yuqi, Luo Zhong, Li Jiang, Hou Xiaojie. Analysis of vibration characteristics of bearing-rotor system considering bolted coupling structure[J]. Journal of Mechanical Engineering, 2019,55(19):60-67.

[11] Li Yuqi, Luo Zhong, Li Jiang, Hou Xiaojie. Uncertainty analysis of axial stiffness of rotor system with bolt connection [J]. Journal of Northeast University (NATURAL SCIENCE EDITION), 2019,40 (05): 700-704 + 721

[12] F.W.D. Tuckmantel, K.L. Cavalca, Vibration signatures of a rotor-coupling-bearing system under angular misalignment, Mech. Mach. Theory 133 (Mar) (2019) 559–583.

[13] R. Ebrahimi, M. Ghayour, H.M. Khanlo, Nonlinear dynamic analysis and experimental verification of a magnetically supported flexible rotor system with auxiliary bearings, Mech. Mach. Theory 121 (Mar) (2018) 545–562.

[14] Yan Qiang. Research on the inspection method of aero-engine bolted rotor assembly tightness [D]. Chang'an University,2019.

[15] Z.Y. Qin, Q.K. Han, F.L. Chu, Bolt loosening at rotating joint interface and its influence on rotor dynamics, Eng. Fail. Anal. 59 (2016) 456–466.

[16] Z.Y. Qin, Q.K. Han, F.L. Chu, Analytical model of bolted disk-drum joints and its application to dynamic analysis of jointed rotor, Proc. Instit. Mech. Eng., Part C: J. Mech. Eng. Sci. 228 (4) (2014) 646–663.